PCCP

PAPER

View Article Online
View Journal | View Issue

Cite this: *Phys. Chem. Chem. Phys.*, 2016, **18**, 29914

First-principles study of relative stability of rutile and anatase TiO_2 using the random phase approximation

Zhi-Hao Cui, Feng Wu and Hong Jiang*

Received 17th July 2016,
Accepted 5th October 2016

DOI: 10.1039/c6cp04973g

www.rsc.org/pccp

The relative stability of TiO_2 in the rutile and anatase structure is wrongly described by density functional theory in various local, semilocal, or even hybrid functional approximations. In this work, we have found that by considering high-order correlations in the adiabatic connection fluctuation–dissipation theory with the random phase approximation (ACFDT-RPA), rutile is correctly predicted to be more stable than anatase, which can be physically attributed to different characters in the electronic band structure of rutile and anatase, including, in particular, that rutile has a smaller band gap than anatase. We further consider the zero-point energy and finite-temperature effects based on the harmonic approximation, and we found that the inclusion of the zero-point energy correction can further increase the relative stability of rutile, and leads to a better quantitative agreement with available experimental measurements. Our study indicates the importance of considering high-order dynamical correlation effects to correctly predict the relative phase stability of polymorphic materials, especially for those systems in which the less stable phase as predicted by conventional local, semilocal or even hybrid density functional approximations has a smaller band gap than the more stable one.

1 Introduction

Titanium dioxide (TiO_2) has become arguably the most important oxide since the discovery of its photocatalytic activity of splitting water to hydrogen and oxygen molecules in early 1970s,[1] and it has been widely utilized in heterogeneous and photo-catalysis[2–4] as well as a lot of other applications.[5] In nature, TiO_2 exists mainly in three polymorphs: rutile, anatase and brookite. The former two are most important, and have been intensively studied. Rutile is the most widely distributed modification of TiO_2 in nature, while anatase is believed to be photocatalytically more active.[6]

First-principles electronic structure theory has played a crucial role in understanding various physical and chemical properties of TiO_2 (see, *e.g.* ref. 7 and references therein). On the other hand, current first-principles approaches have difficulty in predicting correctly the relative stability of the rutile and anatase phases of TiO_2. Experimentally, it has been well established that rutile is thermodynamically the most stable phase (see, *e.g.* ref. 8, for a comprehensive review), which is consistent with the abundance of the rutile TiO_2 mineral in nature.[9–11] In particular, Smith *et al.*[11] recently performed a careful measurement of the thermodynamic properties of TiO_2 in the rutile and anatase phases including their heat capacities in the temperature range from 0.5 K to 1800 K and concluded convincingly that the transformation from anatase to rutile is thermodynamically favorable at all temperatures between 0 and 1300 K. Compared with the experiment, theoretical investigations of the relative stability of the rutile and anatase phases lead to a much more complicated picture. Density-functional theory (DFT) in the local density approximation (LDA) and various generalized gradient approximations (GGA) consistently predicts that anatase is more stable than rutile,[12–14] and no significant improvement can be achieved when using more sophisticated DFT approaches including hybrid functionals (PBE0 and HSE06),[15,16] DFT plus the Hubbard U correction (DFT+U),[15,17,18] and various dispersion-corrected DFT methods.[19,20] It is found that rutile is predicted to be more stable only if the fraction of the exact exchange is greater than 0.78 but smaller than 1.00 when using the HSE-type screened hybrid functional.[15] A similar situation also occurs for the DFT+U method, which predicts rutile to be more stable only if an unphysically large U value is used.

In this work, we address the TiO_2 phase stability issue by first considering the contribution of high-order correlations as accounted for by the adiabatic connection fluctuation–dissipation theorem (ACFDT) with the random phase approximation (RPA).[21–26] The ACFDT-RPA method has been intensively investigated recently

Beijing National Laboratory for Molecular Sciences, State Key Laboratory of Rare Earth Material Chemistry and Application, Institute of Theoretical and Computational Chemistry, College of Chemistry and Molecular Engineering, Peking University, 100871 Beijing, China. E-mail: jianghchem@pku.edu.cn

because of its remarkable performances for molecular and materials systems (see, *e.g.* ref. 25 and references therein). For solids in particular, it can give more accurate prediction about lattice parameters and atomization energies,[27,28] and more importantly it can describe the relative stability of different crystal phases of polymorphic materials much more accurately than conventional density functional approximations.[27,29–32] From a physical point of view, the ACFDT-RPA approach has several attractive features:[24,25] (1) it treats the exchange exactly such that the unphysical self-interaction in the Hartree energy is completely eliminated (we note that the RPA correlation energy itself is not self-interaction error free, but it is a relatively weak effect in most cases[26]), (2) it can correctly describe long-range correlation including, in particular, the van der Waals dispersion interaction, which is the conceptual starting point for recently developed van der Waals density functionals (vdW-DF),[33] and (3) the RPA correlation energy is obtained by a resummation of the so-called "ring" diagrams,[25,34] which takes into account the dynamical screening in a renormalized way and can treat correlation effects in small-gap and metallic systems quite accurately, including static correlation to some extent.[29,35] It is therefore of great interest to investigate whether the consideration of the RPA correction can improve the description of the relative stability of TiO_2. In addition, we also consider the effects of the zero-point energy and finite-temperature vibration of the two TiO_2 phases based on phonon spectroscopy. During the preparation of this paper, Patrick and Thygesen published an article[32] about the DFT+*U*-based RPA approach for the study of the relative phase stability of TiO_2.

The paper is organized as follows. The next section briefly introduces the theoretical approaches used in this work, including the ACFDT-RPA formalism and the finite displacement method for the phonon calculation, and some computational details. In the third section, we first discuss the numerical issue in the RPA calculations related to the accuracy of the PAW pseudopotential to describe high-energy unoccupied states and the convergence with respect to the number of unoccupied states. We then present a systematic investigation of the phase stability of TiO_2 using different theoretical methods, including an in-depth analysis of the relation between the RPA correlation energy and the characteristics in the electronic band structure of rutile and anatase. Section IV summarizes the main findings of this work.

2 Theory and method

2.1 Total energy in the ACFDT-RPA approach

In the ACFDT-RPA approach,[27,28,36] the total energy of a many-electron system can be calculated in terms of the following equation,

$$E_{\text{total}} = T_{\text{KS}} + E_{\text{ion-el}} + E_{\text{H}} + E_{\text{x}} + E_{\text{c}}, \quad (1)$$

where the five terms on the right side are the kinetic energy of the Kohn–Sham (KS) non-interacting system, the electron-nuclear interaction energy, the classical Coulomb repulsion energy among electrons (the Hartree energy), the exact exchange (EXX) energy, and the correlation energy in the random phase approximation, respectively. The latter, in particular, is calculated in terms of

$$E_{\text{c}} = \int_0^\infty \frac{\mathrm{d}\omega}{2\pi} \mathrm{Tr}\{\ln[1 - \chi^0(\mathrm{i}\omega)\nu] + \chi^0(\mathrm{i}\omega)\nu\}, \quad (2)$$

where $\chi^0(\mathrm{i}\omega)$ is the Kohn–Sham response function and ν is the bare Coulomb interaction, both of which are represented in some auxiliary basis.[25] The total energy from the first four terms in eqn (1) is often termed as the EXX total energy, which corresponds to the Hartree–Fock (HF) total energy calculated using KS orbitals instead of self-consistent HF orbitals.

For crystalline systems with $\varepsilon_{n\mathbf{k}}$ and $\psi_{n\mathbf{k}}$ denoting the KS orbital energy and wave functions with the band index n and wave vector $\mathbf{k}$, $\chi^0(\mathrm{i}\omega)$ is calculated by summing over all possible transitions from occupied to unoccupied KS states, which reads, in the planewave representation,[36–38]

$$\chi^0_{\mathbf{G}\mathbf{G}'}(\mathbf{q}, \mathrm{i}\omega) = \frac{1}{V}\sum_{n,n',\mathbf{k}} 2\left(f_{n'\mathbf{k}+\mathbf{q}} - f_{n\mathbf{k}}\right) \times \frac{\left\langle \psi_{n'\mathbf{k}+\mathbf{q}} \middle| \mathrm{e}^{\mathrm{i}(\mathbf{q}+\mathbf{G})\cdot\mathbf{r}} \middle| \psi_{n\mathbf{k}} \right\rangle \left\langle \psi_{n\mathbf{k}} \middle| \mathrm{e}^{-\mathrm{i}(\mathbf{q}+\mathbf{G}')\cdot\mathbf{r}} \middle| \psi_{n'\mathbf{k}+\mathbf{q}} \right\rangle}{\varepsilon_{n'\mathbf{k}+\mathbf{q}} - \varepsilon_{n\mathbf{k}} - \mathrm{i}\omega}, \quad (3)$$

where V is the volume of the unit cell, $f_{n\mathbf{k}}$ is equal to 1 and 0 for occupied and unoccupied states, respectively, and the factor of 2 accounts for the spin degeneracy. Obviously, the RPA correlation energy depends on the KS orbitals used in the calculations, and ideally one should calculate the RPA total energy self-consistently by solving the KS equation with the corresponding exact exchange and RPA correlation potential, which is, however, computationally very expensive, especially for extended systems.[25,39] In this work, we will stay at the non-self-consistent level, and the KS orbitals from different density functional approximations (DFAs), denoted generally as *X*, will be used as the input for RPA calculations, and the corresponding computational scheme is termed as RPA@*X* henceforth.

2.2 The finite displacement approach for the phonon spectrum

The relative stability of different polymorphic phases of a material is often addressed in terms of the ground state total energy,[27,29,31] but generally speaking, other degrees of freedom, including, in particular, those of nuclei vibration, may also play a significant role. The contributions of vibration, including the zero-point energy (ZPE) and finite-temperature vibration enthalpy and entropy, can be obtained from the phonon spectrum calculated in the harmonic approximation. The latter can be obtained by using the finite displacement method[40–42] or density functional perturbation theory (DFPT).[43]

In this work, we use the finite displacement method to calculate the phonon spectrum, from which phonon density of states (ph-DOS) is calculated. In this approach, a supercell is constructed and the forces on each atom in the supercell are

calculated for all possible displacements of the atoms in the primitive cell based on DFT. The supercell should be large enough to ensure that the response of atoms out of the supercell can be neglected. Using α and β to denote Cartesian indices, j and j' as the indices for the atoms in the unit cell, and l and l' as the indices for the primitive cells in the supercell, the force constant matrix elements can be calculated as[41]

$$\Phi_{lj\alpha,l'j'\beta} \approx -\frac{F_{l'j'\beta}(u_{lj\alpha})}{u_{lj\alpha}}, \quad (4)$$

where $F_{l'j'\beta}(u_{lj\alpha})$ is the force on the $l'j'$-th atom in the β direction induced by a small displacement of the lj-th atom in the α direction, $u_{lj\alpha}$, with all other atoms in the supercell fixed in their equilibrium positions. Taking into account the periodicity of the crystal, the dynamical matrix $\mathbf{D}(\mathbf{q})$ can be readily determined as

$$D_{j\alpha;j'\beta}(\mathbf{q}) = \frac{1}{\sqrt{M_j M_{j'}}} \sum_{l'} \Phi_{0j\alpha,l'j'\beta} e^{i\mathbf{q}\cdot(\mathbf{R}_{l'j'}-\mathbf{R}_{0j})}, \quad (5)$$

where $\mathbf{q}$ denotes the phonon wave vector, 0 denotes the primitive cell around the origin, and $\mathbf{R}_{lj}$ denotes the equilibrium position of the lj-th atom. By diagonalizing the dynamical matrix $\mathbf{D}(\mathbf{q})$ as

$$\mathbf{D}(\mathbf{q})\mathbf{e}(\mathbf{q},\nu) = \omega^2(\mathbf{q},\nu)\mathbf{e}(\mathbf{q},\nu), \quad (6)$$

with ν denoting the phonon mode index, one can obtain the phonon energy spectrum $\omega(\mathbf{q},\nu)$, and the corresponding phonon eigenfunctions $\mathbf{e}(\mathbf{q},\nu)$.

Using the phonon energy spectrum, all vibration-related thermodynamic functions, *i.e.* vibrational internal energy (U_{vib}) and entropy (S_{vib}), can be readily calculated as[42]

$$U_{\mathrm{vib}}(T) = \sum_{\mathbf{q},\nu} \hbar\omega(\mathbf{q},\nu)\left[\frac{1}{2} + \frac{1}{\exp(\hbar\omega(\mathbf{q},\nu)/k_{\mathrm{B}}T) - 1}\right], \quad (7)$$

and

$$S_{\mathrm{vib}}(T) = \frac{1}{2T}\sum_{\mathbf{q},\nu} \hbar\omega(\mathbf{q},\nu)\coth(\hbar\omega(\mathbf{q},\nu)/2k_{\mathrm{B}}T) - k_{\mathrm{B}}\sum_{\mathbf{q},\nu}\ln[2\sinh(\hbar\omega(\mathbf{q},\nu)/2k_{\mathrm{B}}T)]. \quad (8)$$

One can then evaluate the enthalpy difference between two different phases at finite temperature (T) and pressure (p) by

$$\Delta H = \Delta E + \Delta U_{\mathrm{vib}}(T) + p\Delta V, \quad (9)$$

where ΔE and ΔV are the difference between the ground state energy and the equilibrium volume of the unit cell per formula unit (f.u.), respectively. We note that for solids at low temperature and normal pressure, the last term in eqn (9) is marginal, and the most important contribution in the second term is that of ZPE.

2.3 Computational details

All DFT calculations including ACFDT-RPA are performed by using Vienna *ab initio* simulation package (VASP)[44] by the projector augmented wave (PAW) method.[45] We have investigated the relative stability of rutile and anatase by using a variety of density functional approximations, including LDA, GGA in the PBE[46] and PBEsol,[47] the TPSS meta-GGA,[48] the vdW functional optB88-vdW[49–52] and the screened hybrid functional HSE06.[53,54] The crystal structures of rutile and anatase TiO_2 are relaxed with a kinetic energy cutoff (ENCUT) of 550 eV for the planewaves, the Γ-centered $\mathbf{k}$-meshes of $6 \times 6 \times 8$ and $6 \times 6 \times 6$ for rutile and anatase, respectively. The energy convergence criterion is 10^{-7} eV and the force convergence criterion is 10^{-4} eV Å^{-1}. To obtain equilibrium lattice constants, we consider a series of unit cell volumes (V), for each of which all internal coordinates and the shape of the unit cell are fully relaxed; the total energy at the equilibrium structure and the bulk modulus are then obtained by fitting the calculated E–V data in terms of the Birch–Murnaghan (B–M) equation of state (EOS).[55,56] Using such a procedure can effectively avoid possible artifacts related to the Pulay stress.[57]

For the ACFDT-RPA calculations, we have tested the convergence of the energy difference between rutile and anatase $\Delta E_{\mathrm{r-a}} \equiv E_{\mathrm{rut}} - E_{\mathrm{anat}}$, which is the main quantity of interest in this work, with respect to key computational parameters including, in particular, the energy cutoff of planewaves and the number of $\mathbf{k}$-points. We have also found a nontrivial dependence of the ACFDT-RPA results on the choice of the PAW pseudopotentials, which is discussed in more detail in the next section. Since structural relaxation using the RPA approach is computationally not feasible due to its demanding computational cost and the lack of analytic forces, we determine the RPA equilibrium lattice constants by calculating the total RPA@X energies at different unit cell volumes with the crystal structures used in the corresponding E–V calculations of the density functional approximation X.

For phonon calculations, the PHONOPY code[42] is used together with VASP with two types of DFAs, LDA and PBEsol. When using the PBE-GGA functional, the original rutile structure is predicted to be unstable and has an imaginary frequency, which is previously reported,[58] and is also reproduced in our study. When using LDA or PBEsol, both rutile and anatase are stable without any imaginary frequency.

3 Results and discussions

3.1 Numerical issue in the ACFDT-RPA approach

Recent studies on the *GW* method (for quasi-particle band structures)[59,60] and the ACFDT-RPA total energy for solids,[60] which all involve the summation over unoccupied states, have established that the accuracy of *GW* and RPA calculations depends on both the accuracy and the completeness of unoccupied states. The former, when using the pseudopotential and planewaves, is determined not only by the energy cutoff for the planewave expansion, but also by the accuracy of the pseudopotentials to describe unoccupied states that are energetically far away from the Fermi level. Currently widely used pseudopotentials, either in the norm-conserving, ultrasoft or PAW schemes, are all optimized mainly for the accurate description of valence states, which may become inadequate for *GW* or RPA calculations, especially for systems with light elements or

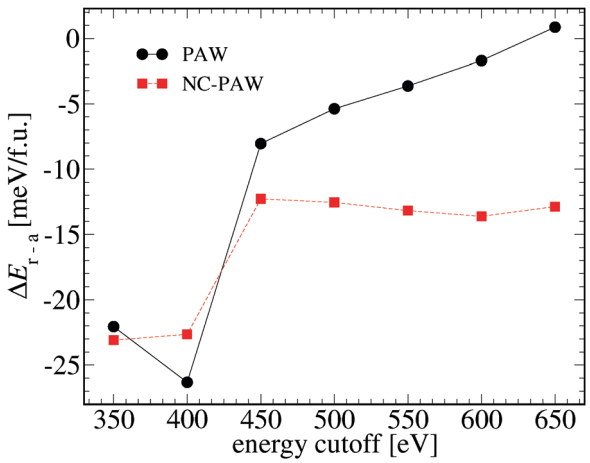

Fig. 1 The convergence of the energy difference between rutile and anatase ΔE_{r-a} per formula unit with respect to the energy cutoff (ENCUT) with the PBE-relaxed crystal structures, calculated using normal PAW and approximately norm-conserving PAW (NC-PAW) pseudopotentials, respectively.

shallow semicore states.[59,60] In the PAW framework, Kresse and coworkers have developed approximately norm-conserving PAW (NC-PAW) pseudopotentials to overcome this problem.[60,61]

To check the effects of the PAW pseudopotentials, we have calculated the total energy difference ΔE_{r-a} between rutile and anatase using two different sets of PAW pseudopotentials, the general purpose PAW pseudopotentials (Ti_sv + O), and *GW*-tuned NC-PAW (Ti_sv_GW + O_GW). The convergences of ΔE_{r-a} with respect to the energy cutoff (ENCUT) of planewaves are shown in Fig. 1. It is remarkable that the convergence behaviors in the two different PAW schemes are dramatically different. When using ENCUT around 400 eV, which is the typical energy cutoff value for normal DFT calculations, the results obtained from PAW and NC-PAW are rather similar. But as ENCUT further increases, ΔE_{r-a} obtained from the normal PAW continuously increases and does not converge even when ENCUT reaches 650 eV, but that obtained using NC-PAW converges well for ENCUT > 450 eV. It is therefore obvious that using the more accurate NC-PAW pseudopotentials is crucial for numerically accurate RPA calculations.

3.2 TiO_2 phase stability by the RPA total energy

Table 1 collects the equilibrium unit cell volumes (V_0) and bulk moduli (B_0) of TiO_2 in the rutile and anatase phases calculated by using different theoretical approaches. In general, it can be seen that the V_0 and B_0 calculated using different approximate exchange–correlation functionals including LDA, GGA (PBE and PBEsol), meta-GGA TPSS and the vdW functional optB88-vdW, are all in good agreement with experiment, and the remaining errors are consistent with the general performances of these different functionals in predicting V_0 and B_0 of solid crystalline systems.[25,68] With regard to the description of the relative stability of rutile and anatase, *i.e.* ΔE_{r-a}, all these approximate functionals predict wrongly that anatase is more stable than rutile. Apparently, when using the van der Waals functional optB88-vdW, ΔE_{r-a} is significantly reduced compared to that obtained using LDA, GGA or hybrid functionals, indicating that the consideration of dynamical correlation in the vdW functional is indeed beneficial to improve the description of the relative phase stability of TiO_2.

Table 1 also collects the results obtained by using the RPA total energy calculated with Kohn–Sham orbitals from different approximate exchange–correlation functionals. To illustrate the effects of considering the RPA correction, we show the B–M EOS curves from PBEsol and RPA@PBEsol as an example in Fig. 2. It is obvious that the consideration of the RPA correction is significant: while PBEsol predicts that anatase is more stable than rutile by 5.95 kJ mol^{-1} f.u.$^{-1}$, RPA@PBEsol reduces the energy difference by 6.34 kJ mol^{-1}, and therefore predicts correctly that rutile is more stable than anatase. As shown in Table 1 and Fig. 3, the RPA results for ΔE_{r-a} depend on the Kohn–Sham orbitals used as the input for the RPA correlation energy, but in all cases, the consideration of the RPA correlation energy predicts correct relative phase stability. Fig. 3 also shows ΔE_{r-a} calculated from the EXX total energy using PBE,

Table 1 The equilibrium volume of the primitive cell V_0, the bulk modulus B_0, the band gap E_g, the energy (ΔE_{r-a}) and enthalpy (ΔH_{r-a}) difference between rutile and anatase obtained from different approaches. The results of ΔH_{r-a} for RPA@PBE and RPA@HSE06 are obtained by using the ZPE correction from the PBEsol calculations, and are therefore included in the parentheses

	V_0 [Å^3]		B_0 [GPa]		E_g [eV]			
Methods	Rut	Anat	Rut	Anat	Rut	Anat	ΔE_{r-a} [kJ mol^{-1}]	ΔH_{r-a} (0 K) [kJ mol^{-1}]
LDA	60.50	66.33	243.5	191.9	1.83	2.06	3.05	
PBE	63.97	70.10	199.1	171.1	1.84	2.12	9.28	
PBEsol	61.98	67.96	220.9	179.6	1.85	2.10	5.95	
HSE06	61.80	67.86	232.9	199.5	3.45	3.73	8.74	
TPSS	63.33	69.67	213.5	174.2			5.87	
optB88-vdW	62.83	68.75	215.7	173.9			1.35	
RPA@LDA	63.60	69.77	219.3	177.0			−0.67	−1.45
RPA@PBE	63.58	69.58	217.4	179.2			−0.09	(−0.93)
RPA@PBEsol	63.59	69.68	218.9	178.1			−0.39	−1.23
RPA@HSE06	62.92	69.14	233.6	188.8			−0.31	(−1.15)
Expt.	62.45[a]	68.13[a]	216[b]	178[c]				−0.42[d], −2.61[e], −1.69[f,g]

[a] Ref. 62. [b] Ref. 63. [c] Ref. 64. [d] Ref. 65. [e] Ref. 66. [f] Ref. 67. [g] Ref. 11.

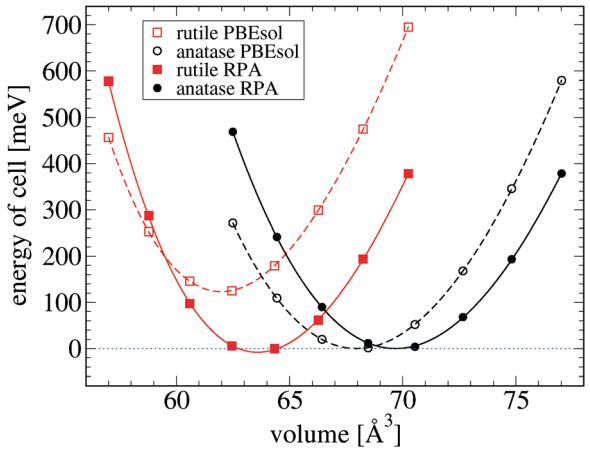

Fig. 2 Equation of state (EOS) curves of rutile and anatase calculated by using the PBEsol and RPA@PBEsol with the total energy of anatase at the equilibrium volume taken as the zero energy.

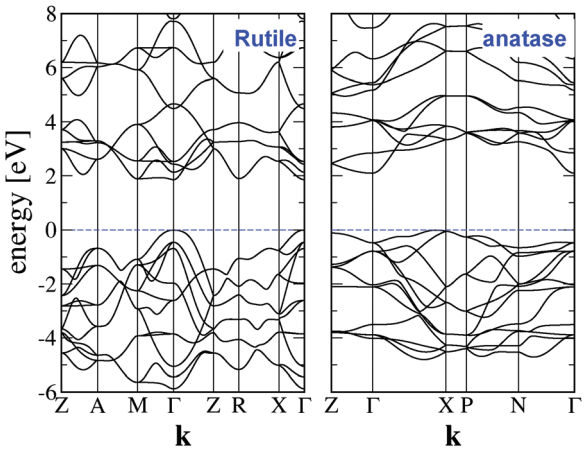

Fig. 4 Band structure of rutile and anatase calculated by PBEsol with the respectively relaxed crystal structures.

PBEsol and HSE06 Kohn–Sham orbitals, and we can see that considering the EXX total energy only would strongly stabilize the anatase phase, indicating that the stability of rutile is mainly determined by correlation effects.

It is of great importance to understand the physical origin for the RPA correlation energy stabilizing rutile. We note from eqn (2) that the RPA correlation energy is calculated from the Kohn–Sham response function that involves a summation over all possible transitions from occupied to unoccupied states (see eqn (3)). The magnitude of the RPA correlation energy is directly related to the energy differences between occupied and unoccupied states that appear in the denominator of eqn (3), which can be characterized by the value of the band gap. We can therefore expect that the magnitude of the band gap has significant effects on the RPA correlation energy, and that systems with smaller band gaps can be more strongly stabilized by considering the RPA correlation energy than those with larger band gaps. Indeed, it is experimentally well established that the band gap of rutile is smaller than that of anatase by about 0.2 eV,[69–71] which is also well reproduced by different theoretical approaches (see, *e.g.* ref. 72) even though their absolute values are significantly underestimated by LDA or GGAs (see the data collected in Table 1).

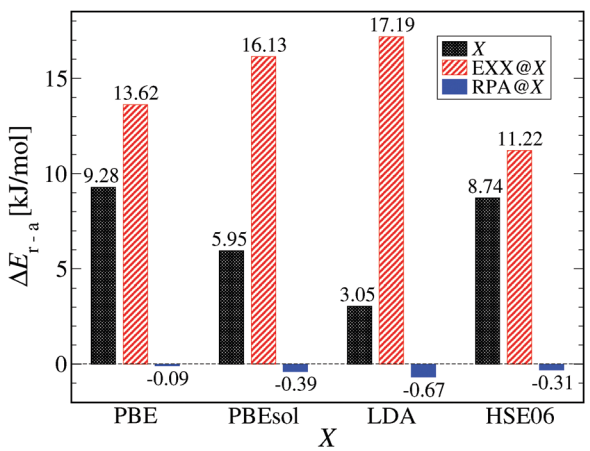

Fig. 3 Total energy difference between rutile and anatase by different methods: *X* (*X* = PBE, PBEsol, LDA, HSE06), EXX@*X* and RPA@*X*.

To see the differences between rutile and anatase more clearly, we show in Fig. 4 the band structure diagram of rutile and anatase calculated using PBEsol in their respectively optimized crystal structures. Two features are most noteworthy. Firstly, the gap between the highest occupied (valence band) state and the lowest unoccupied (conduction band) state, which varies at different wave-vectors (**k**), is overall significantly larger in anatase than in rutile. Secondly, the width of both the valence and conduction bands in rutile is significantly larger than that in anatase, indicating that the inter-atomic orbital overlap is stronger in rutile than in anatase. The latter is consistent with the different structural characteristics of rutile and anatase that rutile is more tightly packed than anatase. The nearest neighboring Ti–Ti distances in rutile are smaller than those in anatase (3.57 and 2.96 Å in the *ab* plane and along the *c* axis in rutile compared to their counterparts in anatase 3.79 and 3.04 Å). To be more specific, each TiO_6 octahedron in rutile is in contact with 10 neighboring octahedra (two by edge sharing and eight by corner-sharing), while each TiO_6 octahedron in anatase is connected to 8 neighboring octahedra (four by edge sharing and four by corner-sharing).[2] In other words, each Ti atom in rutile neighbors more adjacent Ti atoms and in shorter distances than that in anatase. These structural features make the interactions between Ti-3d and O-2p stronger, and therefore results in more significant band dispersion in rutile than in anatase. The latter also means that the matrix elements appearing in the calculation of the Kohn–Sham response function (eqn (3)), which determine the effectiveness of the particular transition concerned, are expected to be more significant in rutile than in anatase.

To see the connection between the RPA correlation energy and the band structure, we show in Fig. 5 the evolution of the **k**-averaged band gap,

$$\bar{E}_g \equiv \frac{1}{N_k}\sum_i (\varepsilon_{c\mathbf{k}_i} - \varepsilon_{v\mathbf{k}_i}), \quad (10)$$

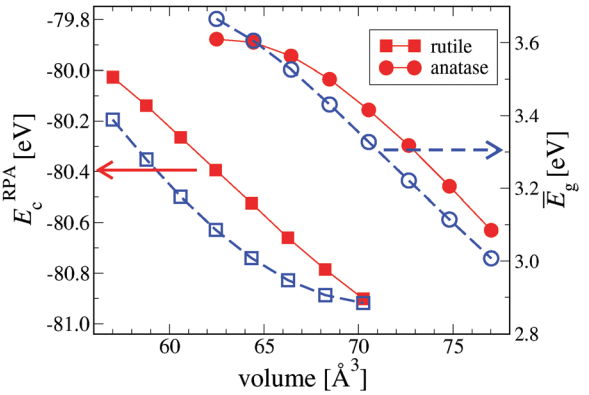

Fig. 5 The RPA correlation energy and the **k**-averaged band gap as a function of the unit cell volume in rutile and anatase.

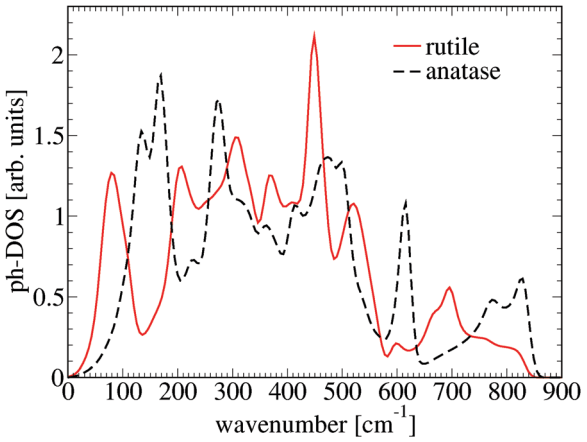

Fig. 6 Phonon DOS in rutile and anatase.

with v and c denoting the indices of the highest occupied valence band and the lowest unoccupied conduction band, respectively, and the RPA correlation energy (E_c^{RPA}) as a function of the unit cell volume in rutile and anatase. When with the same unit cell volume, the **k**-averaged band gap ($\bar{E}_g$) in rutile is about 0.5 eV smaller than that in the anatase. In both phases, as the unit cell volume increases, the band gap decreases, mainly due to the decreasing Madelung potential that plays a dominant role in systems with strong ionic characters.[73] Moreover, the absolute value of the RPA correlation energy increases, which is clearly correlated to the change in the band gap. In particular, when rutile and anatase with different unit cell volumes have similar $\bar{E}_g$, their RPA correlation energies also become very close to each other, which indicates that the magnitude of the RPA correlation energy is strongly correlated to the magnitude of the band gap.

3.3 Zero-point energy correction and temperature effects

In this section, we consider the contribution of the vibration to the relative stability of rutile and anatase. The local structure with the TiO_6 octahedron as the basic building unit is quite similar in rutile and anatase, but the connection between neighboring TiO_6 octahedra is different. As we have mentioned above, rutile has a more tightly packed structure than anatase, based on which we can expect that the two phases can have different phonon features. Fig. 6 shows the phonon density of states (ph-DOS) of rutile and anatase calculated by PBEsol in their respectively optimized crystal structures. Overall, they exhibit qualitatively similar features, but the differences are also quite significant. Approximately each peak in the ph-DOS of rutile is located at lower energy compared to the corresponding one in that of anatase. In particular, the lowest energy peak in rutile ph-DOS appears at about 80 cm^{-1}, which is about 70 cm^{-1} lower than the corresponding peak in the anatase ph-DOS. These differences lead to different zero-point energies in two polymorphs and will favor the stability of rutile due to a smaller vibrational energy.

Using the phonon spectrum calculated above, the enthalpy change for the transformation from anatase to rutile (ΔH_{r-a}) can be calculated at different temperatures and is plotted in Fig. 7.

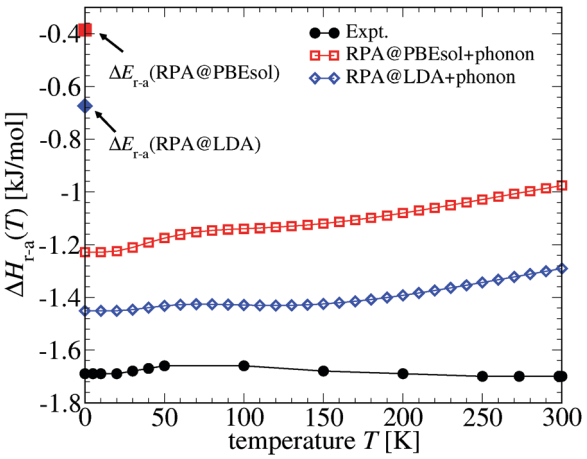

Fig. 7 Zero-point energy effect and temperature dependence. '+phonon' means the method including the zero-point energy effect and temperature influence. The energy differences at 0 K without zero-point energy correction are also plotted in solid points.

The main effect of considering the vibration contribution to the enthalpy is the zero-point energy (ZPE) correction, which differs significantly in rutile and anatase, and stabilizes rutile further by about 0.8 kJ f.u.$^{-1}$ Consistent with previous studies, considering the ZPE correction alone is not enough to reverse the wrong stability order predicted by LDA/GGA or hybrid functionals. But once we have taken into account the correction due to the RPA correlation energy, the consideration of the ZPE correction can further improve the quantitative agreement with the experiment. Considering that the experimental data for the enthalpy difference between rutile and anatase have an error bar of about 0.4–0.9 kJ mol^{-1},[66,67] the agreement between theory and experiment is quite good for all RPA@*X* schemes we have considered. Fig. 7 also shows that the temperature dependence of ΔH_{r-a} is rather weak. On the other hand, the experimentally measured enthalpy depends on the temperature even more mildly. A possible cause for the discrepancy between theory and experiment regarding the temperature dependence is the anharmonicity effect that is not considered in our theoretical calculations.

Using the calculated vibration spectra, we also evaluated the vibration entropy, which is the main contribution to the entropy of solid state systems far below the melting point, to estimate the entropy contribution for the stability of rutile and anatase. At 300 K, the vibration entropy of rutile and anatase is estimated to be 52.06 and 50.81 J K^{-1} mol^{-1}, respectively, resulting in a contribution to the free energy ($T\Delta S$) of 0.38 kJ mol^{-1}, therefore further stabilizing rutile than anatase, which is consistent with previous experimental findings.[11]

3.4 Discussion on the generality of the electronic band structure perspective

Based on the discussion above, we can see that the success of the ACDFT-RPA approach for the prediction of the relative stability of rutile and anatase can be physically attributed to its capability to account for the correlation effects related to the characteristics of the electronic band structure of rutile and anatase, including, in particular, the smaller band gap of rutile than that of anatase. In this section, we will show this can be used as a general perspective to understand the phase stability of other systems.

Graphite *vs.* diamond. It is well known that graphite is more stable than diamond under the low-pressure conditions. However, local or semi-local density functional approximations often have difficulty in predicting the correct stability order. Using the ACFDT-RPA approach, graphite and diamond are predicted to be energetically degenerate after considering the zero-point energy correction.[27] Although it does not fully agree with the experiment quantitatively (graphite is more stable by 5–20 meV than diamond),[27] the improvement is nevertheless remarkable considering that PBE overestimates the stability of diamond by 140 meV. On the one hand, the improvement of RPA can be attributed to its capability to describe the van der Waals interaction between graphene layers correctly. On the other hand, it can also be considered as the band gap difference effect. Graphite is semi-metallic (E_g = 0 eV), while diamond is a wide gap semiconductor (E_g = 5.5 eV), which, based on our preceding analysis, would strongly stabilize graphite.

Cerium (Ce). The Ce metal can undergo an isostructural (fcc) α–γ phase transition with a volume collapse of 15% at room temperature and ambient pressure. It was found in ref. 29 that PBE0 and RPA@PBE0 predict opposite energy orders regarding the two phases: RPA@PBE0 predicts that the low-volume phase is more stable, and PBE0 predicts the opposite. Although this system is metallic, the effects of using the RPA approach can still be understood from the band structure perspective. The low-volume phase has a smaller **k**-averaged band gap (by 0.3 eV based on our HSE06 calculations), which is non-zero even for metallic systems, and therefore the RPA correlation energy will have a stronger stabilizing contribution to the low-volume phase than to the high-volume phase.

There are other systems for which the RPA approach is likely to give a more accurate description of different phases. For example, the relative stability of different allotropes of elemental boron is still an unsolved issue, and there are significant discrepancies between theory and experiment.[74–76] Conventional local or semi-local density functional approximations predict very a similar stability. The differences in the band structures of different allotropes[74] may lead to significantly different high-order correlation energies as described by the RPA approach. On the other hand, the structural complexity of different allotropes of elemental boron makes it highly nontrivial to apply the RPA-like approaches for these materials.

4 Concluding remarks

To summarize, we have reproduced the failure of LDA/GGA and hybrid functionals in the prediction of the relative stability of rutile and anatase. We found that using the state-of-the-art vdW functional (optB88-vdW in particular) can only partially remedy the problem. We have found that the consideration of the ACFDT-RPA total energy in a non-self-consistent way can provide a significant correction to the total energy difference between rutile and anatase, and leads to a qualitatively correct description of their relative stability irrespective of the input Kohn–Sham orbitals used in the RPA calculations. To seek for the origin of the improvement, we have shown that there is a strong correlation between the RPA correlation energy E_c^{RPA} and the band gap, which indicates that the structure with a smaller band gap is more stabilized by considering the RPA correlation energy. We further found that considering the vibrational zero-point energy can further stabilize the rutile phase by about 0.8 kJ mol^{-1}. Combining the corrections from the ACFDT-RPA approach and the zero-point energy effect, we have obtained a quantitative agreement with the experimentally measured enthalpy difference between rutile and anatase.

Compared to conventional LDA/GGAs, or even hybrid functionals, the RPA-like advanced approaches are still computationally very expensive. Recently a lot of efforts have been invested in developing more efficient computational techniques for RPA-type methods,[25,78–80] which, together with continuously increasing computational power, will make these new methods more accessible for more complicated systems. On the other hand, our findings imply that we can use the connection between the characters of the electronic band structure and the RPA correlation energy not only to understand the effects of considering the RPA corrections, but also to obtain some clues on the situations in which using the RPA-like advanced approaches may lead to a significant improvement in the description of the relative stability of different phases. In particular, the RPA-like approach can be especially important for those polymorphic systems in which the less stable phase as predicted by LDA/GGA or the hybrid functional approximations has a smaller band gap than the more stable one. It is, however, important to note that this effect becomes important only if the two competing phases are energetically very close to each other as described by standard DFT calculations. In general, a larger band gap usually means that intra-atomic bonding is stronger, and therefore the structure is more stable. Such cases can be well treated by standard local, semi-local or hybrid functional approximations (see, *e.g.* the relative stability of WO_3 in different polymorphic structures[77]),

and the consideration of the RPA approach would not change the stability order of different phases.[31]

Acknowledgements

This work was partly supported by the National Natural Science Foundation of China (Project No. 21173005, and 21373017, 21321001) and the Ministry of Science and Technology of China (Project No. 2013CB933400). ZHC thanks the support by the Hui-Chun Chin and Tsung-Dao Lee Chinese Undergraduate Research Endowment (CURE).

References

1 A. Fujishima and K. Honda, *Nature*, 1972, **238**, 37.
2 A. Linsebigler, G. Lu and J. Yates, *Chem. Rev.*, 1995, **95**, 735.
3 K. Nakata and A. Fujishima, *J. Photochem. Photobiol., C*, 2012, **13**, 169.
4 X. Chen and S. S. Mao, *Chem. Rev.*, 2007, **107**, 2891.
5 M. Pelaez, N. T. Nolan, S. C. Pillai, M. K. Seery, P. Falaras, A. G. Kontos, P. S. M. Dunlop, J. W. J. Hamilton, J. A. Byrne, K. O'Shea, M. H. Entezari and D. D. Dionysiou, *Appl. Catal., B*, 2012, **125**, 331.
6 S. Na-Phattalung, M. F. Smith, K. Kim, M.-H. Du, S.-H. Wei, S. B. Zhang and S. Limpijumnong, *Phys. Rev. B: Condens. Matter Mater. Phys.*, 2006, **73**, 125205.
7 I. Souza, S. Tosoni and F. Illas, *Chem. Rev.*, 2013, **113**, 4456–4495.
8 D. A. H. Hanaor and C. C. Sorrell, *J. Mater. Sci.*, 2011, **46**, 855–874.
9 T. Mitsuhashi and O. J. Kleppa, *J. Am. Ceram. Soc.*, 1979, **62**, 356.
10 A. Navrotsky and O. J. Kleppa, *J. Am. Ceram. Soc.*, 1967, **50**, 626.
11 S. J. Smith, R. Stevens, S. Liu, G. Li, A. Navrotsky, J. Boerio-Goates and B. F. Woodfield, *Am. Mineral.*, 2009, **94**, 236.
12 J. Muscat, V. Swamy and N. M. Harrison, *Phys. Rev. B: Condens. Matter Mater. Phys.*, 2002, **65**, 224112.
13 F. Labat, P. Baranek, C. Domain, C. Minot and C. Adamo, *J. Chem. Phys.*, 2007, **126**, 154703.
14 P. Mehta, P. A. Salvador and J. R. Kitchin, *ACS Appl. Mater. Interfaces*, 2014, **6**, 3630.
15 M. T. Curnan and J. R. Kitchin, *J. Phys. Chem. C*, 2015, **119**, 21060.
16 V. Swamy and N. C. Wilson, *J. Phys. Chem. C*, 2014, **118**, 8617.
17 M. E. A. Dompablo, A. Morales-García and M. Taravillo, *J. Chem. Phys.*, 2011, **135**, 054503.
18 N. H. Vu, H. V. Le, T. M. Cao, V. V. Pham, H. M. Le and D. Nguyen-Manh, *J. Phys.: Condens. Matter*, 2012, **24**, 405501.
19 J. C. Conesa, *J. Phys. Chem. C*, 2010, **114**, 22718.
20 J. Moellmann, S. Ehrlich, R. Tonner and S. Grimme, *J. Phys.: Condens. Matter*, 2012, **24**, 424206.
21 D. C. Langreth and J. P. Perdew, *Solid State Commun.*, 1975, **17**, 1425.
22 F. Furche, *Phys. Rev. B: Condens. Matter Mater. Phys.*, 2001, **64**, 195120.
23 M. Fuchs and X. Gonze, *Phys. Rev. B: Condens. Matter Mater. Phys.*, 2002, **65**, 235109.
24 H. Jiang and E. Engel, *J. Chem. Phys.*, 2007, **127**, 184108.
25 X. Ren, P. Rinke, C. Joas and M. Scheffler, *J. Mater. Sci.*, 2012, **47**, 7447–7471.
26 H. Eshuis, J. E. Bates and F. Furche, *Theor. Chem. Acc.*, 2012, **131**, 1084.
27 J. Harl and G. Kresse, *Phys. Rev. Lett.*, 2009, **103**, 056401.
28 J. Harl, L. Schimka and G. Kresse, *Phys. Rev. B: Condens. Matter Mater. Phys.*, 2010, **81**, 115126.
29 M. Casadei, X. Ren, P. Rinke, A. Rubio and M. Scheffler, *Phys. Rev. Lett.*, 2012, **109**, 146402.
30 B. Xiao, J. Sun, A. Ruzsinszky, J. Feng and J. P. Perdew, *Phys. Rev. B: Condens. Matter Mater. Phys.*, 2012, **86**, 094109.
31 H. Peng and S. Lany, *Phys. Rev. B: Condens. Matter Mater. Phys.*, 2013, **87**, 174113.
32 C. E. Patrick and K. S. Thygesen, *Phys. Rev. B: Condens. Matter Mater. Phys.*, 2016, **93**, 035133.
33 K. Berland, V. R. Cooper, K. Lee, E. Schröder, T. Thonhauser, P. Hyldgaard and B. I. Lundqvist, *Rep. Prog. Phys.*, 2015, **78**, 066501.
34 A. L. Fetter and J. D. Walecka, *Quantum theory of many-particle systems*, McGraw-Hill, New York, 1971.
35 K. Fuchs, Y. M. Niquet and X. Gonze, *Phys. Rev. Lett.*, 2003, **90**, 189701.
36 J. Harl and G. Kresse, *Phys. Rev. B: Condens. Matter Mater. Phys.*, 2008, **77**, 045136.
37 S. L. Adler, *Phys. Rev.*, 1962, **126**, 413.
38 N. Wiser, *Phys. Rev.*, 1963, **129**, 62.
39 N. L. Nguyen, N. Colonna and S. de Gironcoli, *Phys. Rev. B: Condens. Matter Mater. Phys.*, 2014, **90**, 045138.
40 G. Kresse, J. Furthmüller and J. Hafner, *Europhys. Lett.*, 1995, **32**, 729.
41 D. Alfè, *Comput. Phys. Commun.*, 2009, **180**, 2622.
42 A. Togo and I. Tanaka, *Scr. Mater.*, 2015, **108**, 1.
43 S. Baroni, S. de Gironcoli, A. Dal Corso and P. Giannozzi, *Rev. Mod. Phys.*, 2001, **73**, 515.
44 G. Kresse and J. Furthmüller, *Phys. Rev. B: Condens. Matter Mater. Phys.*, 1996, **54**, 11169.
45 P. E. Blöchl, *Phys. Rev. B: Condens. Matter Mater. Phys.*, 1994, **50**, 17953.
46 J. P. Perdew, M. Ernzerhof and K. Burke, *J. Chem. Phys.*, 1996, **105**, 9982.
47 J. P. Perdew, A. Ruzsinszky, G. I. Csonka, O. A. Vydrov, G. E. Scuseria, L. A. Constantin, X. Zhou and K. Burke, *Phys. Rev. Lett.*, 2008, **100**, 136406.
48 J. Tao, J. P. Perdew, V. N. Staroverov and G. E. Scuseria, *Phys. Rev. Lett.*, 2003, **91**, 146401.
49 M. Dion, H. Rydberg, E. Schröder, D. C. Langreth and B. I. Lundqvist, *Phys. Rev. Lett.*, 2004, **92**, 246401.
50 G. Román-Pérez and J. M. Soler, *Phys. Rev. Lett.*, 2009, **103**, 096102.
51 J. Klimeš, D. R. Bowler and A. Michaelides, *J. Phys.: Condens. Matter*, 2010, **22**, 022201.

52 J. Klimeš, D. R. Bowler and A. Michaelides, *Phys. Rev. B: Condens. Matter Mater. Phys.*, 2011, **83**, 195131.
53 J. Heyd, G. E. Scuseria and M. Ernzerhof, *J. Chem. Phys.*, 2003, **118**, 8207.
54 J. Heyd, G. E. Scuseria and M. Ernzerhof, *J. Chem. Phys.*, 2006, **124**, 219906.
55 F. D. Murnaghan, *Proc. Natl. Acad. Sci. U. S. A.*, 1944, **30**, 244.
56 F. Birch, *Phys. Rev.*, 1947, **71**, 809–824.
57 G. Kresse, M. Marsman and J. Furthmüller, *VASP the guide*, 2016.
58 B. Montanari and N. M. Harrison, *Chem. Phys. Lett.*, 2002, **364**, 528.
59 H. Jiang and P. Blaha, *Phys. Rev. B: Condens. Matter Mater. Phys.*, 2016, **93**, 115203.
60 Y. Hinuma, A. Grüneis, G. Kresse and F. Oba, *Phys. Rev. B: Condens. Matter Mater. Phys.*, 2014, **90**, 155405.
61 A. Grüneis, G. Kresse, Y. Hinuma and F. Oba, *Phys. Rev. Lett.*, 2014, **112**, 096401.
62 K. V. K. Rao, S. V. N. Naidu and L. Iyengar, *J. Am. Ceram. Soc.*, 1970, **53**, 124–126.
63 J. Zhu, J. Yu, Y. Wang, X. Chen and F. Jing, *Chin. Phys. B*, 2008, **17**, 2216.
64 V. Swamy and L. S. Dubrovinsky, *J. Phys. Chem. Solids*, 2001, **62**, 673.
65 C. N. R. Rao, *Can. J. Chem.*, 1961, **39**, 498–500.
66 M. R. Ranade, A. Navrotsky, H. Z. Zhang, J. F. Banfield, S. H. Elder, A. Zaban, P. H. Borse, S. K. Kulkarni, G. S. Doran and H. J. Whitfield, *Proc. Natl. Acad. Sci. U. S. A.*, 2002, **99**, 6476–6481.
67 A. A. Levchenko, G. Li, J. Boerio-Goates, B. F. Woodfield and A. Navrotsky, *Chem. Mater.*, 2006, **18**, 6324–6332.
68 G. I. Csonka, J. P. Perdew, A. Ruzsinszky, P. H. T. Philipsen, S. Lebegue, J. Paier, O. A. Vydrov and J. G. Angyan, *Phys. Rev. B: Condens. Matter Mater. Phys.*, 2009, **79**, 155107.
69 P. A. Cox, *Transition Metal Oxides: An Introduction to their Electronic Structure and Properties*, Clarendon Press, 1992.
70 D. Reyes-Coronado, G. Rodriguez-Gattorno, M. E. Espinosa-Pesqueira, C. Cab, R. de Coss and G. Oskam, *Nanotechnology*, 2008, **19**, 145605.
71 A. Mattsson and L. Österlund, *J. Phys. Chem. C*, 2010, **114**, 14121.
72 H. Jiang, *J. Chem. Phys.*, 2013, **134**, 134115.
73 H. Wang, F. Wu and H. Jiang, *J. Phys. Chem. C*, 2011, **115**, 16180.
74 M. van Setten, G. A. Uijttewaal, M. A. de Wijs and R. A. de Groot, *J. Am. Chem. Soc.*, 2007, **129**, 2458–2465.
75 M. Widom and M. Mihalkovic, *Phys. Rev. B: Condens. Matter Mater. Phys.*, 2008, **77**, 064113.
76 T. Ogitsu, F. Gygi, J. Reed, Y. Motome, E. Schegler and G. Galli, *J. Am. Chem. Soc.*, 2009, **131**, 1903–1909.
77 F. Wang, C. Di Valentin and G. Pacchioni, *J. Phys. Chem. C*, 2011, **115**, 8345–8353.
78 H. Eshuis, J. Yarkony and F. Furche, *J. Chem. Phys.*, 2010, **132**, 132.
79 H.-V. Nguyen and S. de Gironcoli, *Phys. Rev. B: Condens. Matter Mater. Phys.*, 2009, **79**, 205114.
80 M. Del Ben, O. Schütt, T. Wentz, P. Messmer, J. Hutter and J. VandeVondele, *Comput. Phys. Commun.*, 2015, **187**, 120–129.

